Research Article Vol. 59, No. 6 / 20 February 2020 / Applied Optics 1641

Guided terahertz pulse reflectometry with double photoconductive antenna

Mingming Pan,[1] Quentin Cassar,[1] Frédéric Fauquet,[1] Georges Humbert,[2] Patrick Mounaix,[1] and Jean-Paul Guillet[1,*]

[1]IMS Laboratory, University of Bordeaux, UMR 5218, 351 cours de la Libération, 33405 Talence, France
[2]XLIM Research Institute, UMR 7252 CNRS/University of Limoges, 123 av. A. Thomas, 87060 Limoges, France
*Corresponding author: jean-paul.guillet@u-bordeaux.fr

Received 8 November 2019; revised 9 January 2020; accepted 10 January 2020; posted 13 January 2020 (Doc. ID 381646); published 13 February 2020

Developments toward the implementation of a terahertz pulse imaging system within a guided reflectometry configuration are reported. Two photoconductive antennas patterned on the same LT-GaAs active layer in association with a silica pipe hollow-core waveguide allowed us to obtain a guided optics-free imager. Besides working in a pulsed regime, the setup does not require additional optics to focus and couple the terahertz pulses into the waveguide core, simplifying the global implementation in comparison with other reported guided terahertz reflectometry systems. The system is qualified for imaging purposes by means of a 1951 USAF resolution test chart. An image resolution, after a 53 mm propagation length, by about 0.707 LP/mm over the 400–550 GHz integrated frequency band, was obtained, thus providing a promising basis to pursue efforts toward compact guided pulse imagers for sample inspection within the terahertz range.

https://doi.org/10.1364/AO.381646

1. INTRODUCTION

The terahertz frequency region has been attracting an increasing amount of attention over the past decades owing to the abilities of these waves to penetrate opaque structures [1] and to identify specific materials through their spectral features. Relevant technologies such as time-domain spectroscopy (TDS) and THz imaging have been used for various applications [2], e.g., analysis of chemical materials [3], metamaterials [4], biomedical [5], nondestructive testing of composite materials [6,7], art painting [8], or electronics packages [9]. Depending on sample properties, terahertz measurements can be performed either in transmission or in reflection mode. However, the transmitted signal may be too low to be detected for absorbing or thick materials. In this case, a THz system in reflection mode is imperative. Nonetheless, conventional THz sensing systems, using quasi-optic components, only allow us to sense along the optical axis dictated by the optics. Further, the use of optics requires specific longitudinal operating distance, alignment, and minimum volume for implementation. These reflection modalities are not suitable for applications aiming to probe samples directly *in situ*, where the energy dissipation within the whole object cannot be ignored.

To overcome these issues, the use of a waveguide as a single-channel medium both to guide the THz pulse directly to the region of interest and to carry the reflected signal seems to be one solution. Such setups are referred to as guided terahertz reflectometry (GTR) systems. Even though efficient waveguides to forward terahertz waves are yet to be defined, ideal guiding structures should meet specific requirements: first, low losses; second, low dispersion; last, broad frequency bandwidth [10,11]. Throughout the literature, guided reflectometry operations have been realized with different metallic waveguides, including metal wire [12,13] and parallel-plate waveguides (PPWG). Their low dispersion properties in the terahertz regime allow the transmission for a pulse signal. Metal wires have been successfully implemented in terahertz endoscopic systems to probe the bottom of a container [14]. However, this kind of waveguide suffers from poor coupling efficiency and high bending losses, which drastically lessen the power of the transmitted signal. On their part, the fundamental propagation mode of PPWGs can be easily excited with a linear polarization. It has been reported that tapered waveguides could resolve features as small as 100 μm [15]. Nevertheless, the difficulty to maintain the structure remains problematic. Apart from metallic waveguides, the dielectric hollow-core waveguides have been tested as alternative components to develop guided terahertz reflectometry systems. Either a lens or a parabolic mirror is included in the system setup to efficiently couple the terahertz signal into the waveguide. They have been used to analyze the surface state of objects, to determine molecular concentration, and for chemical reaction monitoring [16]. A single-channel flexible waveguide-based terahertz endoscopic

system was demonstrated in 2014 for future clinical application [17]. However, working with optics limits the compactness of such setups. On the other hand, dielectric waveguides are commonly employed in association with continuous sources, but guided pulsed terahertz reflectometry has yet to be investigated.

Here, we report on further developments toward a reflection-mode setup using a double-PCA transceiver in combination with a hollow-core waveguide. We used the TeraSpike TD-800-TR.5 (*Protemics GmbH* Ltd [18]) to generate and detect the terahertz pulses. Compared with two independent devices, each for generation or detection, this transceiver probe, including two PCAs mounted on the same low-temperature growth gallium arsenide (LT-GaAs), is easier to be implemented. Since the LT-GaAs layer carrying two PCAs is deposited at the apex of a slim cantilever (0.18 mm thick and 2 mm wide), the coupling between the transceiver and the waveguide can be achieved without supplemental optics by choosing a suitable waveguide with comparable dimensions. For this reason, a 3 mm diameter hollow-core waveguide was chosen to enable single-channel communication between the transceiver and a sample. The guidance of the waveguide allows us to probe the sample in close proximity and further to perform measurements both through a slight aperture and *in situ* over a large frequency bandwidth.

First, the THz transceiver is characterized to assess its intrinsic properties. The radiation pattern of one of the photoconductive antennas (PCA) is computed by means of a 3D electromagnetic (EM) simulator. In parallel, the silica hollow-core waveguide is tested to determine its working spectral band. Following these investigations, the waveguide is implemented in association with the transceiver to build a guided terahertz pulse reflectometry system. Setup performances for imaging purposes are qualified by imaging a 1951 USAF test target.

2. SETUP

A. Implementation

As depicted in Fig. 1(a), our GTPR system is similar to a TDS setup. Aside from the terahertz transceiver and the waveguide, the system includes some dedicated optics, a mechanical chopper, a lock-in amplifier, and delay line. In combination with the photoconductive receiver on the transceiver, the waveform of a terahertz time signal can be retrieved. While an 800 nm wavelength pump beam excites the emitter from the antenna front side, a probe beam, with similar characteristic, illuminates the transceiver detector from the back side.

When stimulated by the pump laser, photocarriers are generated within the active layer of the photoconductive material. Those carriers are accelerated by an external bias field and thus drive the patterned antenna [19]. Ultimately, the photocurrent is re-emitted as a terahertz pulse. Thanks to adapted dimensions, the terahertz pulses are then injected into the hollow-core waveguide without help of any optics [Fig. 1(b)]. Then, the terahertz signal propagates out of the waveguide and interacts with the sample. A fraction of the emitted signal is reflected back to the waveguide's input facet and reaches the detector on the transceiver probe. Pulse detection is achieved in an analogous way than its emission. The intensity of the induced photocurrent is proportional to the terahertz field that carries the intrinsic dielectric properties of the sample.

B. Transceiver

The two photoconductive antennas are patterned on the same LT-GaAs photoconductive layer, whose thickness is about 1.30 μm. This LT-GaAs layer is located on the apex of a 180 μm thick flexible polyethylene terephthalate (PET) cantilever. Unlike conventional photoconductive antennas using a silicon lens to focus and to collect terahertz pulses, the employed device exploits planar quasi-Yagi antennas to radiate and receive electromagnetic waves. Owning to its great directivity, the use of Yagi antenna has extended from the radio frequency domain to a higher frequency band, up to the optical region.

Terahertz Yagi-Uda antennas depicted in Fig. 1(c) consist of a driven dipole close to the photoconductive switch, a reflector in the rear, and two resonators in front. The radiation pattern of the antennas has been evaluated by a 3D electromagnetic

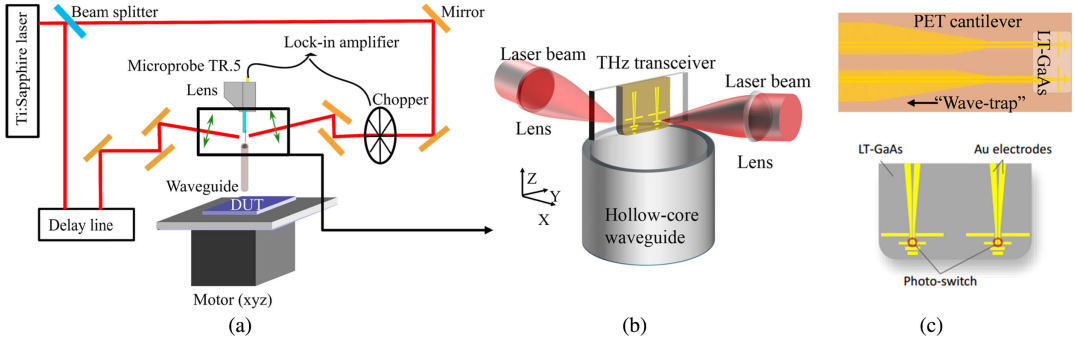

Fig. 1. Description of guided terahertz wave reflectometry system setup. (a) Global view of the experimental setup, which is equivalent to a standard TDS system, but with the difference being that two focused laser beams are injected on a single chip containing two antennas. The generated wave is then transmitted via the waveguide to the device under test (DUT); then, one fraction of the incident signal comes back through the same waveguide to the other PC antenna acting as detector. (b) Close-up view between the double photoconductive antennas and the waveguide. Back face illumination was preferred for one of the PC antennas to avoid congestion issues from the lenses. Since the LT-GaAs layer dimensions are comparable with the diameter of the waveguide core, the generated signal is expected to be directly coupled into the waveguide. (c) Top: Schematic view of the PET cantilever. The "wave-trap" design along the two electrode lines is supposed to avoid the overlap of reflections from the sample and probe itself. Bottom: Close-up view of the transceiver probe tip. Two photoconductive switches with Yagi-Uda antennas are deposited on the LT-GaAs layer.

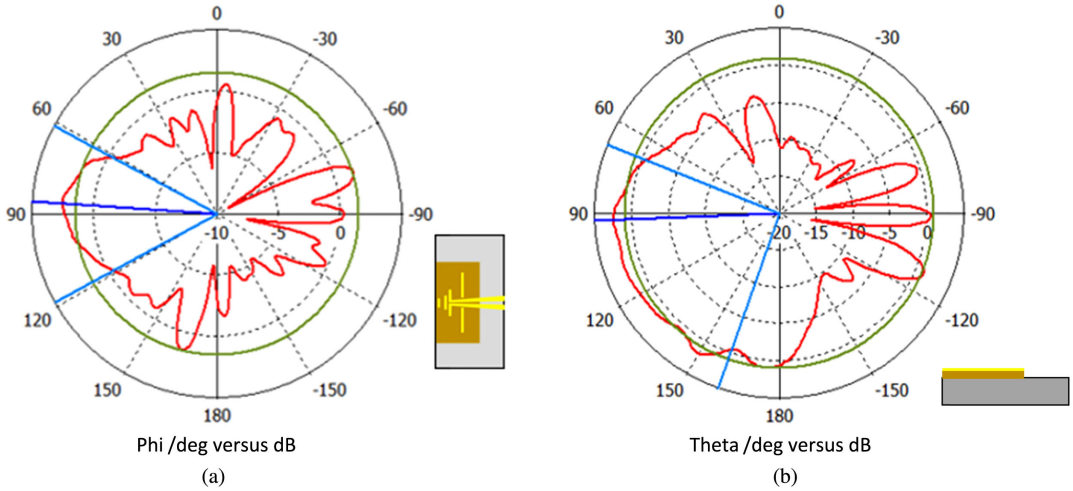

(a) (b)

Fig. 2. 2D radiation pattern at 400 GHz, calculated by the EM simulator CST. (a) Directivity of antenna when theta = 90° (E-plane). Phi = 86° is the main lobe direction, toward the front of antenna. (b) Directivity of antenna when phi = 90° (H-plane). Theta = 92° is the main lobe direction, toward the front of antenna. Besides, we can observe that the radiated wave is more toward the substrate.

simulator (CST Microwave Studio) (2D polar diagrams are depicted in Fig. 2).

The E-plane exhibits a main lobe (Phi = 86°) oriented in the direction of the antenna, which corresponds to the typical response of the Yagi–Uda antenna [20]. Impacted by the high refractive index of the substrate, the generated waves tend to radiate into free space toward the substrate, which was demonstrated in the polar diagram along the H-plane [shown in Fig. 2(b)]. Besides, the back lobe in the radiation pattern reveals that an important fraction of generated signal propagates toward the transceiver base. It may produce some unwanted echoes from the transceiver base back to the PCA. Thus, perpendicular lines, called *wave-traps*, are patterned on the transceiver metallic lines to reduce the internal reflections and hence to avoid the superposition of reflected signals from the two opposite directions [21]. In the case that two PCAs are presented on the LT-GaAs layer, their side lobes (shown in the radiation pattern along the E-plane) lead to a direct communication between them. In order not to assign this direct transmission as a result of the interaction between the emitted radiations and the sample, a metal sheet acting as a perfect mirror was placed directly below the transceiver with varying distance of 2 mm [shown in Fig. 3(a)]. Two contributors have then been recorded: first, the signal arising from the direct transmission between the two antennas; second, the reflections occurring at the metallic plate surface. While the first contribution, attributed to the cross-talk effect, remains consistent for different mirror distances, signals due to the reflection from the metallic plate obviously exhibit time delay and amplitude decrease with increasing distances. In addition, compared with the direct transmitted signal between two PCAs whose spectral width extends from 200 GHz to 1.2 THz, reflections from the metallic surface present a useful bandwidth up to 700 GHz mainly limited by the low total radiation efficiency of the antenna at high frequency [shown in Fig. 3(b)].

C. Hollow-Core Waveguide

Because the distance between the two photoconductive antennas is around 700 μm, the waveguide to be implemented within a guided pulse terahertz reflectometry system has to have a comparable diameter size to realize an optics-free single-channel communication. Dielectric hollow-core waveguides exploit the antiresonant effect as a guiding mechanism. The high-index cladding layer acts as a Fabry–Perot cavity, while the low-index core allows the terahertz wave propagation at noncharacteristic frequencies. The characteristic frequencies of the cladding are defined by [22,23]

$$f_m = \frac{mc}{2t\sqrt{n^2-1}}, \tag{1}$$

where c is the speed of the light in vacuum, m is an integer, and t and n are the thickness and refractive index of the cladding, respectively. Low-loss propagations within the waveguide are expected owing to the low absorption of terahertz frequencies in air core of the waveguide. In view of the foregoing, a silica pipe hollow-core waveguide with a diameter of 3 mm and a thickness of 130 μm has been chosen. In such a selected case, $t = 130$ μm and $n = 1.97$. Characteristic frequencies of the silica cladding are expected to be around 687 GHz, 1.37 THz, and 2.06 THz. By using a fiber TDS system (TPS4000, TeraView Ltd., Cambridge UK), two waveguides with different lengths (201 and 301 mm, respectively) have been characterized in transmission-mode configuration. Because the incident beam size from the terahertz source is bigger than the dimension of the waveguide, a polyethylene lens is inserted between the emitter and the waveguide to facilitate the coupling. As indicated in Fig. 4, the dips in the spectrum of the transmitted signal correspond appropriately to calculated resonant frequencies, confirming the waveguide's guiding mechanism. Moreover, the exhibited waveguide behavior reports relatively large carrying bandwidth from 350 up to 650 GHz. As a consequence, such a guiding structure matches the supported frequency band,

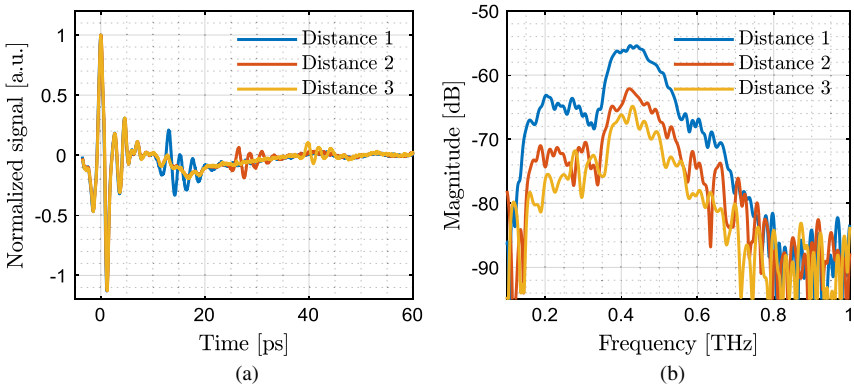

Fig. 3. Detected signals with different distances between the transceiver and metal sheet (2 mm step). (a) Time domain signal. There is an overlapped part among different measurements (for example, when $t = [0 - 10]$ ps), which corresponds to a reference signal obtained by the cross-talk between the emitter and the detector. (b) Spectrum of the signal reflected by the metal in a varying distance. As the propagation distance increases, reflections become weaker. The transceiver has successfully detected these reflections, and it is more sensitive to the frequencies between 200 and 700 GHz.

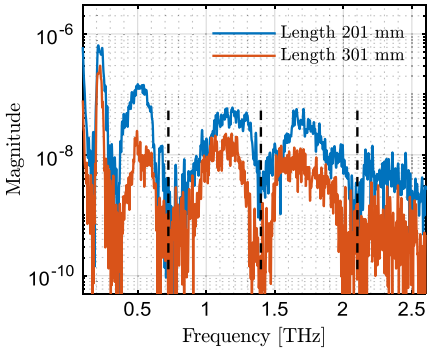

Fig. 4. Spectrum of the transmitted signals via silica hollow-core waveguides with different lengths. (Blue curve: 201 mm length waveguide; red curve: 301 mm length waveguide.) The expected resonant frequencies of silica cladding ($f = 687$ GHz, 1.37 THz, and 2.06 THz) are marked with the vertical dash–dot lines. The corresponding attenuation peaks in the spectrum demonstrate that this waveguide exploits the antiresonant reflections as a guiding mechanism.

thus enabling a simple coupling setup and low dielectric loss expectations [24].

D. Full Setup 3D Simulation

In order to estimate the portion of energy transferred from the terahertz transceiver to the waveguide core, an FDTD simulation was performed. The energy density was successively calculated at two distinct sections: first, the surface directly subsequent to the end of the transceiver (S_1); second, the interface section between free space and the waveguide, located 900 μm from the transceiver (S_2). The energy density transfer between the transceiver to the waveguide was then determined as

$$\eta(f) = \frac{\iint_{S_2} \frac{1}{2}\varepsilon_0\varepsilon_r |E_{\text{in}}(x, y, z)|^2 \mathrm{d}x\mathrm{d}y}{\iint_{S_1} \frac{1}{2}\varepsilon_0\varepsilon_r |E_{\text{out}}(x, y, z)|^2 \mathrm{d}x\mathrm{d}y} \tag{2}$$

where S_1 and S_2 are the respective sections onto which are summed the energy fractions and where E_{in} and E_{out} stand for the energy entering the waveguide and emitted by the transceiver, respectively. The energy density coupled to the waveguide as a function of the frequency is depicted in Fig. 5. The maximum transfer has been found at 340 GHz with an efficiency by about 22.78%, while the lowest transfer is located at 490 GHz with a respective efficiency of 13.25%. Further simulations were performed to assess the propagation of the terahertz pulses along the waveguide. To this aim, a metal plate was numerically placed at the end of the waveguide to maximize the back-end reflection, which is not displayed in the simulation model given in Fig. 6(a). The absolute value of the electric field at various propagation time is shown in Fig. 6(b). At $t = 10$ ps, the wave appears at the photoconductive antenna emitter then propagates to the end of the waveguide. Figure 6(c) displays the signal measured at the second antenna port. From 0 to 25 ps, the recorded signal corresponds to the direct communication between the two antennas. From 25 to 50 ps the signal corresponds to the reflected portion at the entrance of the hollow-core waveguide. The signal reflected from the back end is recorded from $t = 360$ ps. Finally, as shown in Fig. 6(d), focus is given to the reflected signal, which consists of several main oscillations and of higher modes propagating more slowly in the high-index cladding layer.

3. EXPERIMENTAL RESULTS

A. Time Domain Result

The benefits of wave guiding lie in the fact that terahertz waves can reach farther targeted sites of inspection while minimizing energy dissipation in comparison with free space propagation. This aspect was verified by measuring the reflected signal from a metal plate situated 53 mm from the terahertz transceiver (just below the waveguide's output). The reflected signal was hence compared between free space propagation to that of a guided regime. Results are reported in Fig. 7, including originally detected signals (a) and reflected signals from sample (b) after removing the direct transmission signal between two PCAs.

As expected from a guiding structure, guided terahertz pulses exhibit a significantly higher amplitude compared with that

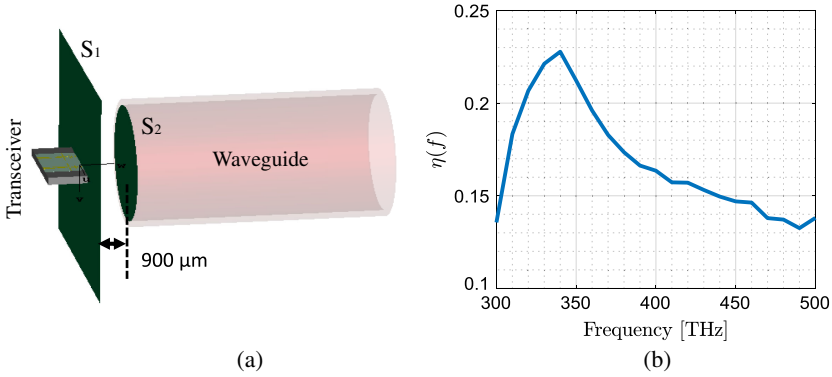

Fig. 5. (a) Model of the transceiver probe and hollow-core waveguide in CST. The distance between the transceiver probe tip and the waveguide is 900 μm. While the first rectangle section is placed at the probe tip of the transceiver to calculate the radiated energy by the transceiver, the second circle section lies at the input facet of the waveguide to evaluate the received energy. (b) By comparing the energy passing through two sections, the portion directly injected into the waveguide can be obtained.

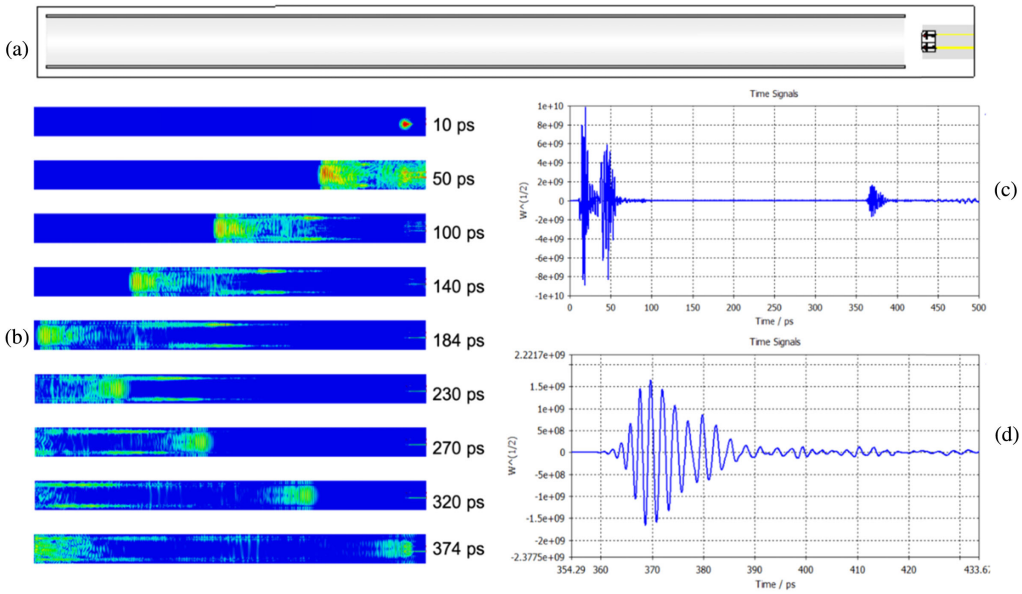

Fig. 6. Full simulation of the setup. (a) Scheme of the model. (b) Cross-section along the waveguide of the absolute value of the electric field at different time of simulation. (c) Reflected signal obtained at the detector PCA port. (d) Zoom on the signal correspond on the reflection at the end of the waveguide.

of nonguided ones. The power fraction carried by reflected pulses propagating through the hollow-core waveguide is roughly 12 dB greater than that of those propagating in free space for frequencies spanning from 400 to 650 GHz [shown in Fig. 7(c)]. Such a working frequency band is mainly determined by the terahertz transceiver response and the waveguide propagation modes. Nevertheless, the reflected signal propagating through the waveguide is impacted by signal distortions in the time domain.

B. Imaging Results

After the demonstration of an effective terahertz pulse guidance, we focus on the reflection imaging capabilities of this system. As represented in Fig. 8(a), a positive 1951 USAF resolution test target is placed just below the output of waveguide (a distance less than 0.5 mm). The scanned zones cover elements in group −1 and −2, which are indicated by red rectangles. By moving the 1951 USAF test chart, a raster scan is performed to record the time signal at each point. A pixelated data map is eventually constructed. An image can be obtained both in time or the frequency domain by different mathematical criteria [25]. For example, by integrating frequency components from 400 to 550 GHz, two images have been extracted [Figs. 8(b) and 8(c)]. Line profiles of terahertz magnitude along the solid line AB in group −2 and line A′B′ in group −1 are additionally provided. The resolution is given in pairs of lines (a transparent and a reflective) per millimeter (pl/mm) or in thickness of the corresponding line. When the contrast between bars and substrate is lower than 0.3, it is estimated that two stripes cannot be differentiated. Therefore, lines are still clearly distinguished until the element 4 in group −1. The width of a line is about 707 μm,

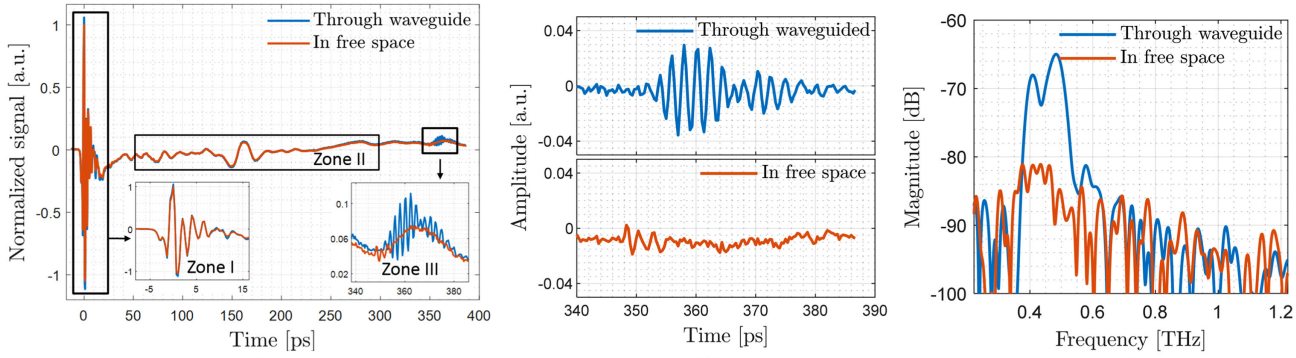

Fig. 7. (a) Detected signals by the terahertz transceiver. Blue curve: Signal propagating through the waveguide. Red curve: signal propagating in air (baseline). We divided this signal into three zones. First, zone I ($t = [0 - 30]$ ps) corresponds to the cross-talk between the two photoconductive antennas; it can be obtained even without the sample. Then, zone II ($t = [30 - 250]$ ps) corresponds to reflection signal coming from probe mount and imperfection of wave trapping design [16]. Finally, in zone III (after 340 ps), we observe the reflected signal from the sample at the end of the waveguide (blue curve) and a weak reflected signal by free propagation (red curve). (b) Pure reflections from metal in the time domain. (c) Spectrum of reflection signals obtained at Fig. 7. (b). It demonstrates that more signal power is transmitted compared with free propagation owning to the guidance of glass waveguide.

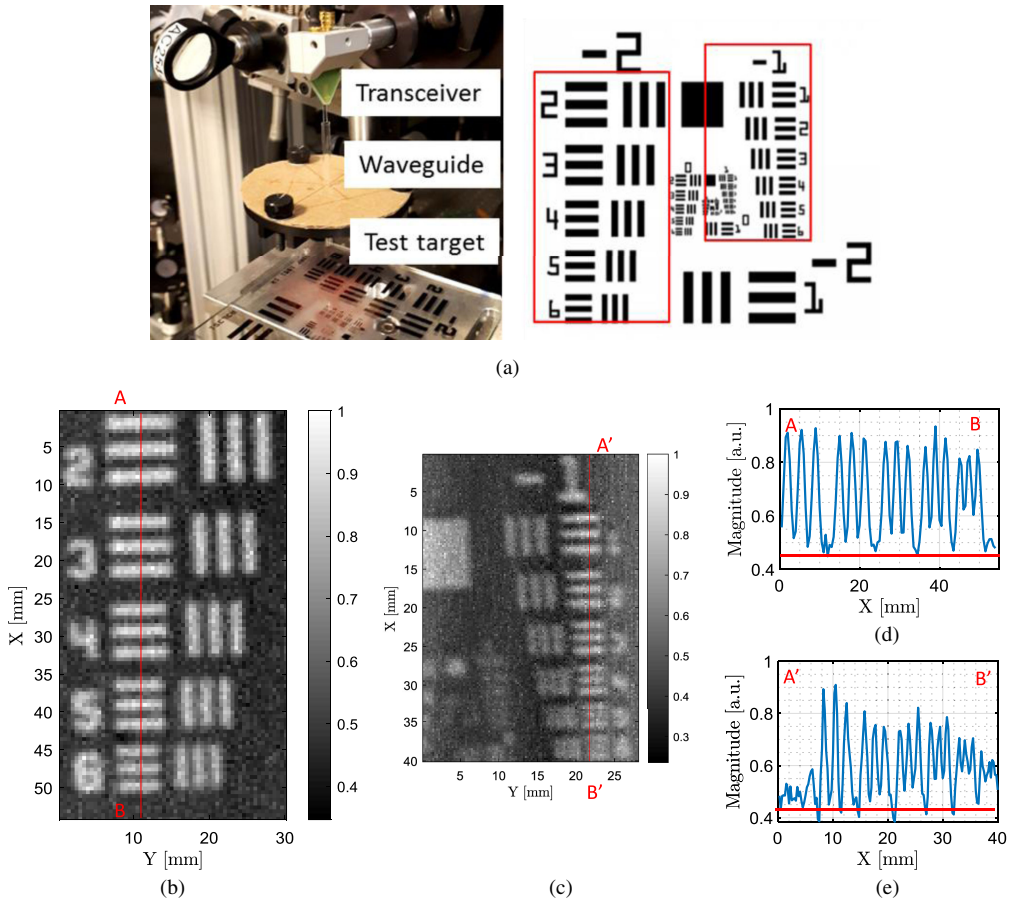

Fig. 8. (a) Left: Photography of experimental setup. The silica hollow-core waveguide is placed below the terahertz transceiver, and a 1951 USAF test target as sample is mounted on the linear translation stages. Right: 1951 USAF test target image, in which the scanned areas are marked by the red rectangles. (b) and (c) Two images of the scanned areas (elements in group −1 and in group −2, respectively) are obtained from the trapezoidal integration between 400 and 550 GHz. (d) and (e) Line profiles of terahertz field magnitude along the solid line AB in group −2 and solid line A′B′ in group −1.

and the spatial frequency is about 0.707 LP/mm. The imaging performance is mainly limited by the nonperfect frequency match among the transceiver and the waveguide, the laser noise, and the mechanical constraints of motorized stage.

4. CONCLUSION

In this work, a guided terahertz pulse reflectometry system has been successfully constructed by taking advantage of a terahertz waveguide and a transceiver. The generation and detection of terahertz radiations are realized by using a terahertz transceiver, while terahertz waves are guided by a waveguide. The silicon lens, beam splitter, or coupler is no longer required to manipulate the terahertz beam in free space, which makes this system setup more compact and easier to align. In the future, an integrated system with an antenna and waveguide could be convenient for terahertz imaging experiments having spatial issues.

Funding. Ministère de l'Education Nationale; de l'Enseignement Supérieur et de la Recherche.

REFERENCES

1. D. M. Sheen, D. L. McMakin, and T. E. Hall, "Three-dimensional millimeter-wave imaging for concealed weapon detection," IEEE Trans. Microw. Theory Tech. **49**, 1581–1592 (2001).
2. S. S. Dhillon, M. S. Vitiello, E. H. Linfield, and E. Al, "The 2017 terahertz science and technology roadmap," J. Phys. D **50**, 043001 (2017).
3. J. A. Zeitler, P. F. Taday, D. A. Newnham, M. Pepper, K. C. Gordon, and T. Rades, "Terahertz pulsed spectroscopy and imaging in the pharmaceutical setting – a review," J. Pharm. Pharmacol. **59**, 209–223 (2007).
4. O. Mitrofanov, F. Dominec, P. Kužel, J. L. Reno, I. Brener, U.-C. Chung, C. Elissalde, M. Maglione, and P. Mounaix, "Near-field probing of Mie resonances in single TiO_2 microspheres at terahertz frequencies," Opt. Express **22**, 23034–23042 (2014).
5. U. R. Pfeiffer, P. Hillger, R. Jain, J. Grzyb, T. Bücher, Q. Cassar, G. MacGrogan, J.-P. Guillet, P. Mounaix, and T. Zimmer, "Ex vivo breast tumor," IEEE Microw. Mag. **20**(9), 32–46 (2019).
6. Q. Cassar, A. Chopard, F. Fauquet, J.-P. Guillet, M. Pan, J.-B. Perraud, and P. Mounaix, "Iterative tree algorithm to evaluate terahertz signal contribution of specific optical paths within multi-layered materials," IEEE Trans. Terahertz Sci. Technol. **9**, 684–694 (2019).
7. F. Friederich, K. May, B. Baccouche, C. Matheis, M. Bauer, J. Jonuscheit, M. Moor, D. Denman, J. Bramble, and N. Savage, "Terahertz radome inspection," Photonics **5**, 1 (2018).
8. C. L. K. Dandolo, J.-P. Guillet, X. Ma, F. Fauquet, M. Roux, and P. Mounaix, "Terahertz frequency modulated continuous wave imaging advanced data processing for art painting analysis," Opt. Express **26**, 5358–5367 (2018).
9. E. Kowalczuk, A. Bhattacharya, K. C. Lee, E. Alton, J. Alton, M. Igarashi, and S. Barbeau, "Fault localisation of defects using electro optical terahertz pulse reflectometry and 3D EM modelling with virtual known good device," in *International 3D Systems Integration Conference (3DIC)* (2014), pp. 1–4.
10. S. Atakaramians, V. S. Afshar, T. M. Monro, and D. Abbott, "Terahertz dielectric waveguides," Adv. Opt. Photon. **6**, 293–339 (2014).
11. H. Bao, K. Nielsen, O. Bang, and P. U. Jepsen, "Dielectric tube waveguides with absorptive cladding for broadband, low-dispersion and low loss THz guiding," Sci. Rep. **5**, 7620 (2015).
12. J. P. Guillet, L. Chusseau, R. Adam, T. Grosjean, A. Penarier, F. Baida, and D. Charraut, "Continuous-wave scanning terahertz near-field microscope," Microw. Opt. Technol. Lett. **53**, 580–582 (2011).
13. L. Chusseau and J.-P. Guillet, "Coupling and propagation of Sommerfeld waves at 100 and 300 GHz," J. Infrared Millim. Terahertz Waves **33**, 174–182 (2012).
14. K. Wang and D. M. Mittleman, "Metal wires for terahertz wave guiding," Nature **432**, 376–379 (2004).
15. M. Awad, M. Nagel, and H. Kurz, "Tapered Sommerfeld wire terahertz near-field imaging," Appl. Phys. Lett. **94**, 051107 (2009).
16. B. You and J.-Y. Lu, "Remote and in situ sensing products in chemical reaction using a flexible terahertz pipe waveguide," Opt. Express **24**, 18013–18023 (2016).
17. P. Doradla, K. Alavi, C. Joseph, and R. Giles, "Single-channel prototype terahertz endoscopic system," J. Biomed. Opt. **19**, 080501 (2014).
18. Protemics, "TeraSpike TD-800-TR.5," http://www.protemics.com/index.php/products/teraspike/td-800-tr.
19. E. Castro-Camus and M. Alfaro, "Photoconductive devices for terahertz pulsed spectroscopy," Photon. Res. **4**, A36–A42 (2016).
20. H. Yagi and S. Uda, "Projector of the sharpest beam of electric waves," Proc. Imp. Acad. **2**, 49–52 (1926).
21. B. Guo, "Revealing the truth about 'Trapped Rainbow' storage of terahertz waves in plasmonic grating," Plasmonics **13**, 933–938 (2017).
22. C. Lai, B. You, J. Lu, T. Liu, J. Peng, C. Sun, and H. Chang, "Modal characteristics of antiresonant reflecting pipe waveguides for terahertz waveguiding," Opt. Express **18**, 309–322 (2010).
23. E. Nguema, D. Férachou, G. Humbert, J. Auguste, and J. Blondy, "Broadband terahertz transmission within the air channel of thin-wall pipe," Opt. Lett. **36**, 1782–1784 (2011).
24. J.-Y. Lu, C.-P. Yu, H.-C. Chang, H.-W. Chen, Y.-T. Li, C.-L. Pan, and C.-K. Sun, "Terahertz air-core microstructure fiber," Appl. Phys. Lett. **92**, 064105 (2008).
25. H. Balacey, B. Recur, J.-B. Perraud, J. B. Sleiman, and P. Mounaix, "Advanced processing sequence for 3-D THz imaging," IEEE Trans. Terahertz Sci. Technol. **6**, 191–198 (2016).